INSTITUTE OF PHYSICS PUBLISHING MODELLING AND SIMULATION IN MATERIALS SCIENCE AND ENGINEERING

Modelling Simul. Mater. Sci. Eng. **11** (2003) 745–753 PII: S0965-0393(03)64097-0

Molecular dynamics simulations of stress-induced phase transformations and grain nucleation at crack tips in Fe

A Latapie and D Farkas

Department of Materials Science and Engineering, Virginia Polytechnic Institute and State University, Blacksburg, VA 24061-0237, USA

Received 15 August 2002, in final form 28 May 2003
Published 4 July 2003
Online at stacks.iop.org/MSMSE/11/745

Abstract

The molecular dynamics simulation technique is used to study a stress-induced new grain formation mechanism at the crack tip of a nanocrystalline α-iron sample at temperatures ranging from 100 to 600 K. The stress-induced formation of new bcc grains, created inside existing grains, is found to occur through a metastable bcc to fcc phase transformation at the crack tip of the sample. A Nishiyama–Wassermann orientation relationship is found between the original bcc grain and the fcc phase and a Kurdjumov–Sachs orientation relationship is found between the new bcc grain created and the fcc transition phase. The new grain nucleation is observed to increase with increasing temperature and stacking faults associated with the fcc phase are observed at the higher temperatures.

1. Introduction

Fracture and deformation mechanisms in nanocrystalline materials have been the subject of intensive research for the last two decades. The evolution of the crack tip under increased stress intensity is fundamental for the understanding of fracture mechanisms and toughness in nanocrystalline materials. For these materials, fracture process and deformation mechanisms are thought to be different from those for conventional grain size polycrystalline materials. Because of the extremely small size of the grains, mechanisms such as dislocation generation and multiplication or dislocation pile-up at the grain boundaries are no longer supported. Thus, fracture and plastic deformation are thought to occur by intergranular mechanisms instead of a dislocation-based fracture process. At such small grain sizes, mechanisms such as grain boundary sliding, grain rotation and grain boundary triple junction activity have been proposed to account for plastic deformation without dislocation motion [1–6].

Many studies have been performed in recent years to explore the atomistic processes of crack propagation in bcc α-iron [7–16]. These studies have largely stressed the mechanisms

of crack propagation in α-iron single crystals. However, very few results have been published on nanocrystalline α-iron [17–19]. Reference [20] presents an atomistic simulation study on the deformation and fracture mechanisms in nanocrystalline Ni. The fracture process is observed to proceed as an intragranular fracture process combined with some degree of plasticity. Deformation mechanisms are found to occur by grain boundary accommodation and sliding. A study of the elastic behaviour of nanocrystalline α-iron was performed recently [21], showing the variation of elastic constants that results from extremely small grain sizes.

The stress-induced nucleation of a closely packed grain in α-iron has been observed previously in a single crystal simulation study by Kadau *et al* [22]. In that study, multimillion atom molecular dynamics (MD) simulations were used to investigate the shock-induced phase transformation from the bcc structure of an Fe single crystal to a closed packed structure. The orientational relations between the transformed and untransformed regions were found to be similar to those found for temperature-driven martensitic transformations in Fe and its alloys. A similar structural transition from bcc to hcp structures was observed by Nishimura *et al* [23] in single and bicrystal systems.

Crack propagation in Fe single crystals has been studied previously [11] and the results show dislocation emission when the crack lies on {011} plane with the front parallel to either a $\langle 110 \rangle$ or a $\langle 111 \rangle$ direction. The $[011](01\bar{1})$ crack emits pure edge dislocations with $\frac{1}{2}\langle 111 \rangle$ Burgers vectors on {211} slip planes, inclined at 54.73° with the crack plane. The $[1\bar{1}1](110)$ crack emits dislocations with $\frac{1}{2}\langle 111 \rangle$ Burgers vectors on {110} planes, inclined at 60° with the crack plane. The emitted dislocations are not restricted from moving away from the crack tip and are found to be piled up against the boundary of the simulation cell. Nishimura and Miyazaki [23] observed the nucleation of the hcp phase for a crack on a {101} type plane propagating along a $\langle 010 \rangle$ type direction.

In this study, we describe the grain nucleation and growth mechanism that has been observed during a mode I fracture process of a simulated nanocrystalline α-iron sample. We observed this strain induced grain nucleation mechanism ahead of the crack tip in a nanocrystalline α-iron sample at different temperatures (100, 300 and 600 K). With increasing stress intensity loading on the simulated nanocrystalline sample, the crack propagation within a grain is not associated with dislocation emission at the crack tip. Instead, a stress-induced metastable region ahead of the crack tip nucleates into a new grain that grows as the stress intensity loading is increased. The new grain created has the same stable bcc structure as the original grain, but a different crystallographic orientation. The process of grain formation and crystallographic orientation relationships between the original grain and the new grain created are described in this study. The new grain is nucleated with the aid of a transformation to a close-packed phase similar to that observed by Kadau *et al* [22] Furthermore, the grain formation mechanisms are observed to be temperature dependent.

2. Computational technique

Atomistic computer simulation and particularly MD simulation is a very useful technique to study the fracture mechanisms in metallic materials [24–28]. The approach yields very detailed information about the simulated systems. For the purpose of this study, a nanocrystalline sample was geometrically created using the Voronoi construction [29, 2, 20]. In this construction, grains are randomly nucleated within a cube. Each grain grows with a random crystallographic orientation until the grains reach one another, generating grain boundaries. The Voronoi construction gives a random nanocrystalline sample with a grain boundary structure similar to what is expected in polycrystalline materials. These grain boundaries have

been characterized in detail [30, 31]. The sample created contained 15 grains and 2 000 000 atoms, which gives an average grain size of 12 nm.

The sample was then relaxed into a stable nanocrystalline α-iron structure using molecular statics (MS) along with the embedded atom method (EAM) potential from Simonelli *et al* [32] to describe the atomic interactions in α-iron. A comparison of this potential with other interatomic potentials available in the literature can be found in a previous paper [33]. The potential was fitted to the cohesive energy of the bcc phase (4.28 eV) as well as the vacancy formation energy and elastic constants of the bcc phase. The fcc phase is predicted to be less stable that the bcc phase by 0.03 eV. The surface energy along the {110} type plane was found to be 1.424 J m^{-2}. This potential was used previously in a MS simulation of crack propagation in an α-iron single crystal [11]. Using a conjugate gradient approximation method [34], the minimum energy state is reached through an iterative relaxation process. The energy is computed after each iteration and the system is assumed to be at equilibrium when the forces on each atom are below a specified value.

A semi-infinite mode I crack was introduced in the α-iron sample using the isotropic elastic approximation. MS was used to relax the crack tip region to a minimum energy configuration. Periodic boundary conditions are used in the direction of the crack front. The initial crack is an atomically sharp wedge with its tip located near the centre of the simulation block. The cracked sample was equilibrated at three different temperatures (100, 300 and 600 K) using MD for 2000 steps (each step is 8×10^{-15} s). With the same technique, the fracture process was conducted for the three temperatures by incrementally loading the semi-infinite mode I crack starting from a stress intensity value slightly below the Griffith criterion value for a single crystal (0.6 eV Å$^{-5/2}$ = 0.96 MPa $\sqrt{\text{m}}$). For the nanocrystal, the Griffith value is expected to be lower by up to 30%, due to the contribution of the grain boundary energy. We let the system evolve for 1000 MD steps between each loading (each step is 8×10^{-15} s), giving an overall simulation time of 200 ps (25 000 steps). Under the stress intensity at a certain temperature, the sample evolves according to the equations of motion. Since the MD technique follows the actual forces on the atoms, the fracture mechanisms can be determined by direct observation, without having any *a priori* assumptions. As the simulation progresses and the stress intensity loading is increased, the crack begins to advance and we follow the crack for a stress intensity up to three times the Griffith value. The visualization of the fracture process is made possible by cutting slices along the crack front line of the sample. The simulated strain rate is very high compared with real experiments, and because of this limitation we conducted MS simulations of the same samples to compare them with MD simulations at low temperature. We verified that the same fracture and deformation mechanisms occur using the conjugate gradient technique, representative of a rate that allows equilibrium to be reached at each loading level.

3. Results

For all the temperatures tested (100, 300 and 600 K), at an early stage of the stress intensity increase, the crack tip advance is associated with a localized metastable phase ahead of the crack tip within different grains along the crack front line. Figures 1(*a*) and (*b*) illustrate the early stage of the transformation at the crack tip, at 8 ps and 56 ps, respectively. The bcc orientation of the original grain transforms into a localized region with a different atomistic structure. To clearly represent the atomic structure of the sample, a colour code associated with the atomic arrangement of the atoms is adopted. The atoms in perfect bcc arrangement (eight-coordinated atoms) are coloured in green. The atoms with less than eight neighbours are coloured in red. Therefore, the atoms that belong to the crack surface are all red. Finally, the atoms with more than eight neighbours are coloured in blue. This nomenclature allows

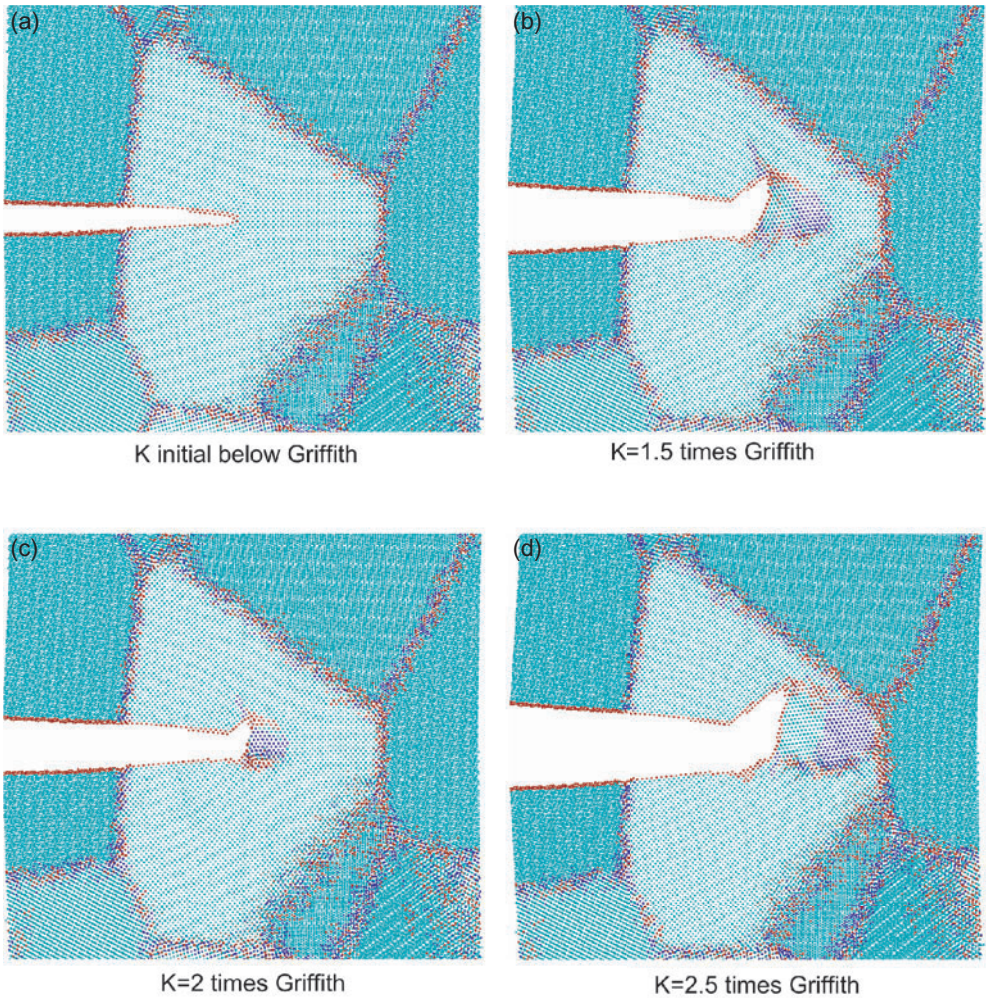

Figure 1. FCC transformation and grain nucleation ahead of the crack tip at 100 K as the loading is increased, shown for (*a*) 8 ps, (*b*) 56 ps, (*c*) 104 ps and (*d*) 152 ps.

us to distinguish grain boundaries, with atoms not perfectly ordered, from inner grains, with atoms in perfect bcc arrangement, and from eventual defects due to deformation and fracture mechanisms. Hence, in figure 1, the zone coloured in blue ahead of the crack tip illustrates a phase transformation from bcc to a phase with atoms with higher coordination number. Detailed analysis showed this phase to be fcc.

As the stress intensity is increased, the crack keeps propagating in the most favourable crystallographic orientation and the fcc region becomes more important ahead of the crack tip. With increasing stress intensity, part of the fcc region closer to the crack tip is transformed back to a more stable bcc structure (figures 1(*c*) and (*d*) for 104 ps and 152 ps, respectively). The fcc structure is only 0.03 eV atom^{-1} higher in energy than the bcc structure according to this potential. The bcc region formed from the fcc phase does not have the same crystallographic orientation as the original bcc grain. Figure 2 illustrates the three different regions ahead of the crack tip, where the fcc region in blue constitutes the transition between the original bcc

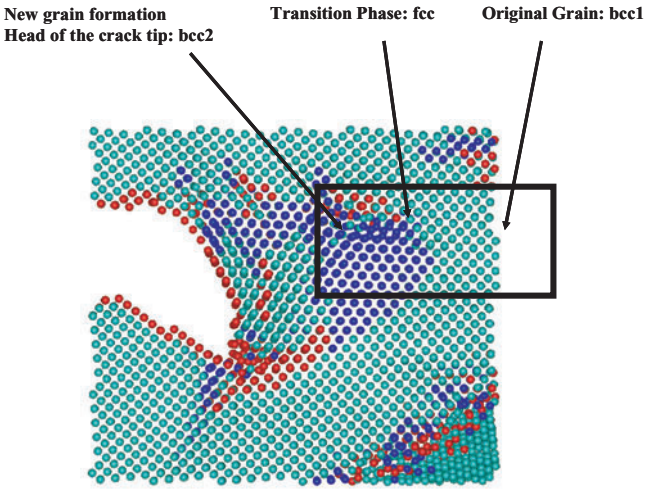

Figure 2. FCC transition phase from original bcc grain to newly created bcc2 grain.

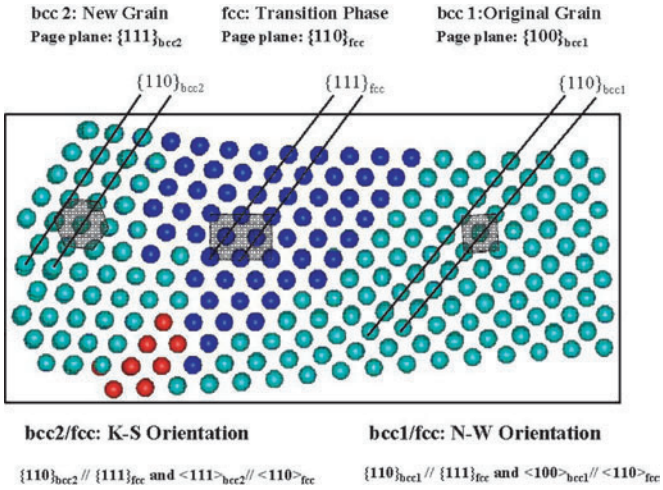

Figure 3. Orientation relationships between bcc1, fcc and bcc2.

grain (bcc1) and the newly formed bcc grain (bcc2). Specific crystallographic orientation relationships exist between these regions. Figure 3 shows an enlargement of the relevant region of figure 2 and describes the orientation relationships between the different regions. It is seen that the orientation relationship between the fcc structure and the original bcc grain is very close to $(110)_{bcc1}//(111)_{fcc}$ and $[100]_{bcc1}//[110]_{fcc}$. This bcc–fcc orientation relationship coincides with the well known Nishiyama–Wassermann [35] orientation relationship. On the other hand, the orientation relationship between the fcc phase and the newly created bcc grain is very close to $(110)_{bcc2}//(111)_{fcc}$ and $[111]_{bcc2}//[110]_{fcc}$, which corresponds to the well known Kurdjumov–Sachs [36] orientation relationship. With increasing stress intensity, the newly created bcc grain grows from the fcc phase. Once the new bcc grain is created from the fcc phase, a grain boundary is formed between the new bcc grain and the original grain. The grain boundary created is close to a pure twist grain boundary in a $\{110\}$ plane. The new bcc

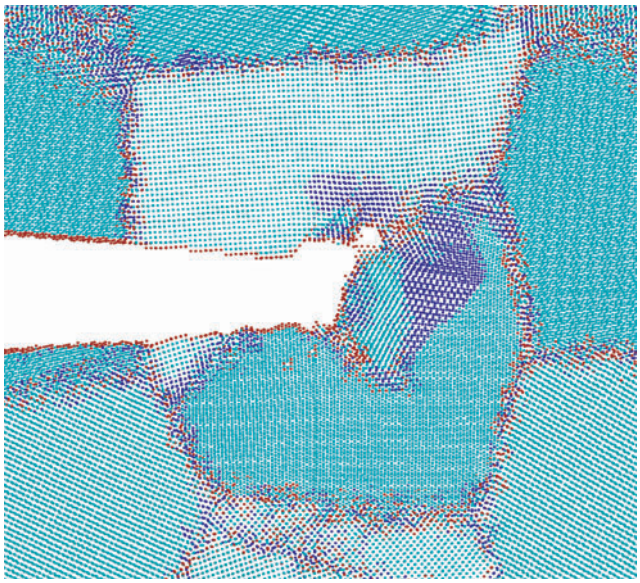

Figure 4. Grain nucleation at a different location in the sample at 600 K.

grain has rotated about 45° around a ⟨110⟩ axis from the original grain within the {110} grain boundary plane.

The same type of phenomenon is observed in different parts of the sample but always in the inner region of the grains. The process is found to be temperature dependent. As we increase the temperature from 100 to 600 K, more nucleation sites for new grains are observed in different regions of the sample. Figure 4 shows another grain formation through the same type of phase transformation mechanism at 600 K in a different grain than the one studied previously. The orientation relationships between the different phases are found to be the same. Indeed we observe a bcc–fcc Nishiyama–Wassermann orientation relationship between the original bcc grain and the fcc phase and a Kurdjumov–Sachs orientation relationship between the new bcc grain created and the fcc phase (figure 5). The increase in temperature is associated with increasing presence of stacking faults in the transitional fcc phase. At 100 K, the fcc region is free from stacking faults, which are only observed at 300 and 600 K. Figure 6 illustrates the stacking fault observed in the fcc region between the original bcc grain and the nucleated bcc grain at 600 K. The stacking faults in the fcc region at 300 and 600 K are believed to be the consequence of the emission of Shockley partial dislocations from the crack tip into the transitional fcc region. Temperature and grain size are found to highly influence the fracture mechanisms. From direct observations of the fracture process, it is clear that the increase in temperature causes more blunting and crack arrest. We also observe more grain nucleation sites associated with crack propagation at higher temperatures. With increasing temperature, the atomic vibrations increase causing atoms to move more easily when subjected to loading. Thus, at higher temperature plastic deformation becomes easier and crack blunting occurs. This is true for the various mechanisms of plastic deformation observed, namely dislocation emission, grain boundary sliding, stress-induced phase tranformation and the nucleation of new grains. From these atomistic observations, fracture resistance is increased with increasing temperature, as expected.

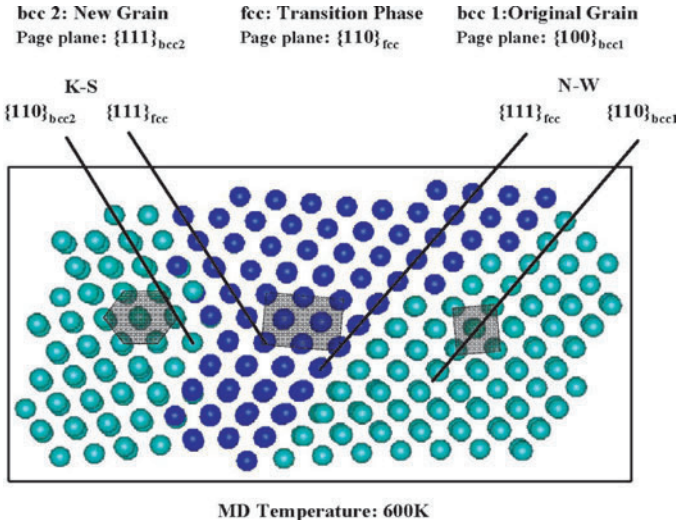

Figure 5. Orientation relationships between bcc1, fcc and bcc2 at 600 K.

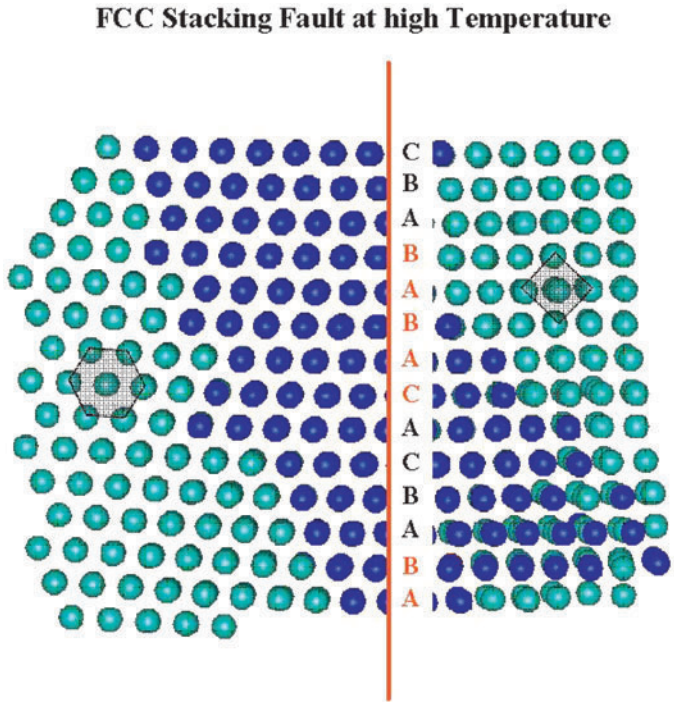

Figure 6. Stacking fault illustration in the fcc region at 600 K.

4. Conclusions

The plastic deformation at the crack tip of the nanocrystalline α-iron studied is not associated only with dislocation emissions but also with phase transformations and new grain nucleation. The stress at the crack tip is released by atomic reorganization instead of dislocation emissions.

Thus the bcc1 to fcc to bcc2 transformation observed is a stress-induced mechanism accounting for plastic deformation at the crack tip of the sample. This mechanism of grain nucleation and grain growth is part of the deformation mechanisms observed during the crack propagation in nanocrystalline α-iron. Along with grain boundary accommodation, grain rotation and grain boundary triple junction activity, the mechanism of new grain formation dictates the energy release mechanisms in nanocrystalline α-iron with temperatures ranging from 100 to 600 K. We observed that characteristic orientation relationships, such as Kurdjumov–Sachs and Nishiyama–Wasserman, exist between the newly created grain, the fcc phase and the original grain. Furthermore, the increase in temperature is associated with more grain nucleation sites that account for more plastic deformation in the nanocrystalline sample.

Experimental studies reveal that under certain pressure and temperature combinations, phase transformations in bcc iron occur. For instance, at a pressure greater than 10 GPa, iron possesses a hexagonal close-packed structure [37,38]. At high temperatures, both bcc and hcp phases transform into an fcc structure [39]. For a certain range of pressure and temperature, the bcc structure of iron is found to transform into a reversible fcc structure [40]. Other experimental observations have shown nano grain formation associated with stress-induced phase transformation in steel [41]. Also, atomistic simulation studies have demonstrated stress-induced phase transformations in α-iron [8,42]. In particular [42] addresses a reversible bcc to fcc stress-induced phase transformation in α-iron. In our study, we observed a similar reversible bcc to fcc stress-induced phase transformation. With increasing loading, the stress intensity at the crack tip induces a local bcc to fcc transformation. It is important to underline that the fcc structure is only $0.03\,\mathrm{eV\,atom^{-1}}$ higher in energy than the bcc structure according to this potential. High stress intensity at the crack tip induces the bcc to fcc transformation, but eventually this high-energy configuration goes back to a more stable structure, where the fcc region transforms back to a bcc structure, creating the new bcc grain. This can consitute a mechanism of grain rotation. Haslam *et al* [43] combined MD simulations with mesoscale simulations to elucidate the mechanism and kinetics of grain growth in nanocrystalline materials. These simulations demonstrate that grain growth can also be triggered by the coordinated rotations of neighbouring grains to eliminate the common grain boundary between them. The mechanism reported here can therefore have a significant influence in grain growth kinetics in nanocrystalline materials. The use of MD was motivated by the ability of the technique to reproduce the physical behaviour of the system. Since the MD technique follows the actual forces on the atoms as they migrate, the fracture mechanisms can be determined by direct observation, without having any *a priori* assumptions. However, it is important to stress that from a quantitative point of view, the accuracy of this technique is limited by the accuracy of the potentials used.

Acknowledgments

This work was supported by the office of Naval Research, Division of Materials Science (Grant Number N00014J-1351). We specially acknowledge the help of Helena van Swyngehoven with the codes and techniques for the creation of polycrystalline digital samples. We also acknowledge helpful discussions with W T Reynolds.

References

[1] Schiotz J, Di Tella F and Jacobson K 1998 *Nature* **391** 561
[2] Van Swygenhoven H, Spaczer M and Caro A 1999 *Acta Mater.* **47** 3117
[3] Hasnaoui A, Van Swygenhoven H and Derlet P M 2002 *Phys. Rev.* B **66** 184112

[4] Van Swygenhoven H and Derlet P M 2001 *Phys. Rev.* B **64** 224105
[5] Hahn H and Padmanabhan K A 1997 *Phil. Mag.* B **76** 559
[6] Palumbo G, Erb U and Aust K 1990 *Scr. Metall. Mater.* **24** 2347
[7] Cheung K and Yip S 1994 *Modelling Simul. Mater. Sci. Eng.* **2** 865
[8] Cheung K S, Harrison R J and Yip S 1992 *J. Appl. Phys.* **71** 4009
[9] deCelis B, Argon A and Yip S 1983 *J. Appl. Phys.* **54** 4864
[10] Kohlhoff S, Gumbsch P and Fischmeister H F *Phil. Mag.* A **64** 851
[11] Shastry V and Farkas D 1996 *Modelling Simul. Mater. Sci. Eng.* **4** 473
[12] Machova A, Beltz G E and Chang M 1999 *Modelling Simul. Mater. Sci. Eng.* **7** 949
[13] Ogawa K 1965 *Phil. Mag.* **11** 217
[14] Mullins M 1984 *Acta Metall.* **32** 381
[15] Vitek V 1970 *Scr. Metall.* **4** 725
[16] Yanagida N and Watanabe O 1996 *JSME Int. J.* A **39** 321
[17] Inoue H, Akahoshi Y and Harada S 1995 *Mater. Sci. Res. Int.* **1** 95–9
[18] Chen D 1995 *Mater. Sci. Eng.* A **190** 193–8
[19] Chen Z and Ding J 1998 *NanoStructured Mater.* **10** 205
[20] Farkas D, Van Swyngehoven H and Derlet P 2002 *Phys. Rev.* B **66** 060101
[21] Latapie A and Farkas D 2003 *Scr. Metall. Mater.* **48** 611
[22] Kadau K, Germann T C, Lohmdahl P S and Holian B L 2002 *Science* **296** 1681
[23] Nishimura K and Miyazaki N 2001 *CMES-Comput. Model. Eng. Sci.* **2** 143
[24] Farkas D 2000 *MRS Bull.* **25** 38
[25] Zhou S J, Beazley D M and Lomdahl P S and Holian B L 1997 *Phys. Rev. Lett.* **78** 479
[26] Cheung K S and Yip S 1990 *Phys. Rev. Lett.* **65** 2804
[27] Kalia R K, Nakano A, Omeltchenko A, Tsuruta K and Vashishta P 1997 *Phys. Rev. Lett.* **78** 2144
[28] Farkas D 2000 *Phil. Mag. Lett.* **80** 229
[29] Voronoi G 1908 *Reine Angew. Math.* **134** 199
[30] Van Swygenhoven H, Farkas D and Caro A 2000 *Phys. Rev.* B **62** 831
[31] Derlet P M and Van Swygenhoven H 2003 *Phys. Rev.* B **67** 014202
[32] Simonelli G, Pasianot R and Savino E 1993 *Mater. Res. Soc. Symp. Proc.* **291** 567
[33] Farkas D, Zhou S J, Vailhe C, Mutasa B and Panova J 1997 *J. Mater. Res.* **12** 93
[34] Sinclair J E and Fetcher R 1972 *J. Phys.* C **7** 864
[35] Nishiyama Z 1934 *Sci. Rep. Ser.* 1 **638** (Tohoku University, Sendai)
[36] Kurdjumov G and Sachs G 1930 *Z. Phys.* **64** 325
[37] Jamieson J C and Lawson A W 1962 *J. Appl. Phys.* **33** 776
[38] Mao H K, Bassett B A and Takahashi T 1967 *J. Appl. Phys.* **38** 272
[39] Bundy F P 1965 *J. Appl. Phys.* **36** 616
[40] Zhang J and Guyot F 1999 *Phys. Chem. Minerals* **26** 419
[41] Fujiwara H, Inomoto H, Sanada R and Ameyama K 2001 *Scr. Mater.* **44** 2039
[42] Najafabadi R and Yip S 1983 *Scr. Metall.* **17** 1199
[43] Haslam A J, Moldovan D, Phillpot S R, Wolf D and Gleiter H 2002 *Comp. Mat. Sci.* **23** 15